Phosphorus Diffusion Mechanisms and Deep Incorporation in Polycrystalline and Single-Crystalline CdTe

Eric Colegrove,[1] Steven P. Harvey,[1] Ji-Hui Yang,[1] James M. Burst,[1] David S. Albin,[1] Su-Huai Wei,[2] and Wyatt K. Metzger[1]

[1]*National Renewable Energy Laboratory, 15013 Denver West Parkway, Golden, Colorado 80401, USA*
[2]*Beijing Computational Science Research Center, Beijing 100193, China*

(Received 27 January 2016; published 19 May 2016)

A key challenge in cadmium-telluride (CdTe) semiconductors is obtaining stable and high hole density. Group-I elements substituting Cd can form acceptors but easily self-compensate and diffuse quickly. For example, CdTe photovoltaics have relied on copper as a dopant, but this creates stability problems and hole density that has not exceeded 10^{15} cm^{-3}. If hole density can be increased beyond 10^{16} cm^{-3}, CdTe solar technology can exceed multicrystalline silicon performance and provide levelized costs of electricity below conventional energy sources. Group-V elements substituting Te offer a solution, but they are very difficult to incorporate. Using time-of-flight secondary-ion mass spectrometry, we examine bulk and grain-boundary diffusion of phosphorus (P) in CdTe in Cd-rich conditions. We find that in addition to slow bulk diffusion and fast grain-boundary diffusion, there is a critical fast bulk-diffusion component that enables deep P incorporation in CdTe. Detailed first-principle calculations indicate the slow bulk-diffusion component is caused by substitutional P diffusion through the Te sublattice, whereas the fast bulk-diffusion component is caused by P diffusing through interstitial lattice sites following the combination of a kick-out step and two rotation steps. The latter is limited in magnitude by high formation energy, but is sufficient to manipulate P incorporation. In addition to an increased physical understanding, these results open up experimental possibilities for group-V doping in CdTe applications.

DOI: 10.1103/PhysRevApplied.5.054014

I. INTRODUCTION

P-type doping in II-VI materials is critical for a variety of semiconductor devices, but this can be challenging for certain materials such as cadmium telluride (CdTe). Intrinsic p-type doping with cadmium vacancies (V_{Cd}) is limited due to its high acceptor energy, and the necessary Te-rich stoichiometry decreases the formation energy of harmful midgap recombination centers such as Te antisites (Te_{Cd}) [1]. Extrinsic doping is also difficult. Group-I dopants tend to self-compensate, and while they can be incorporated at low temperatures due to fast diffusion, the fast diffusion also creates stability issues and self-compensation that can limit hole density [1–5]. Furthermore, these elements form somewhat deep acceptors [6], 100–200 meV above the valance band, which can reduce lifetime [7,8] in addition to the lifetime reducing midgap states associated with Te-rich stoichiometry. In CdTe solar technology, the use of Cl and Cu as dopants or passivants has failed to produce hole density greater than 10^{15} cm^{-3} and contributed to the stagnation of open-circuit voltage (V_{OC}) for 30 years [9–11]. If this problem can be overcome, CdTe solar technology can outperform multicrystalline silicon with a levelized cost of electricity below fossil fuels [12]. Recent results have indicated that CdTe with group-V dopants placed substitutionally on the Te lattice sites can achieve radiatively limited lifetimes and hole concentrations exceeding 10^{17} cm^{-3} [13]. Early data also suggest that group-V dopants appear to remain more stable [8]; however, incorporating these elements is more difficult.

It is critical to establish a strong understanding of defect energetics and kinetics as new defect chemistries are needed for next-generation applications. This work focuses on the diffusion of phosphorus (P) under Cd-rich conditions in single-crystal (sX) and thin-film polycrystalline (pX) CdTe by studying samples annealed for different temperatures and times. P on a Te site (P_{Te}) has an ionization energy of about 60 meV [14–16], which is suitable for p-type doping, and recent sX devices utilizing P have achieved a V_{OC} larger than 1000 mV [13]. Yet, despite their importance, there have been limited diffusion kinetic studies for group-V elements in CdTe. Hall and Woodberry published some P diffusion and incorporation data in the 1960s [17], followed more recently by Hoonnivathana *et al.* [18]. Based on the diffusion coefficients they reported for single crystals, it would appear that bulk P diffusion is too slow to achieve meaningful incorporation at temperatures viable for solar module production. Diffusion results for group-V elements in pX CdTe materials have not been published. Here, we combine diffusion experiments on both sX and pX CdTe with three-dimensional (3D) profiles of P concentration from time-of-flight secondary-ion mass spectroscopy (TOF-SIMS) to derive bulk and grain-boundary (GB) diffusion parameters.

We observe the slow bulk diffusion from earlier work, report on GB diffusion kinetics in *pX* material, and observe an important fast bulk-diffusion component that enables deep P incorporation in the bulk at relatively low temperatures. First-principles calculations give an atomistic theoretical description for each observed diffusion mechanism.

II. EXPERIMENT AND METHODS

CdTe single crystals and *pX* thin films are used as the base semiconductor material for this work. The single crystals are commercially available and nominally undoped with 100 orientation (JX Nippon Mining & Metals Corp.). The *pX* thin films are fabricated on molybdenum-coated alumina substrates by close-spaced sublimation (CSS) in a hydrogen ambient. The films are deposited to a thickness of about 30 μm, and subsequently polished mechanically to 25 μm to reduce effects of surface roughness on measurements and analysis. The grain size at these polished surfaces is 13–14 μm. The *sX* and *pX* samples are placed in evacuated and sealed quartz ampoules with a source powder that supplied a constant P and Cd overpressure throughout anneals in a three-zone furnace (MELLEN, Inc.). Based on previously reported diffusion coefficients, samples are annealed at different temperature and times to maintain the bulk-diffusion length near one of two values (see Table I). This is done to diffuse enough P into each sample to be easily measurable, keep the sample set of reasonable size, and anneal at different temperatures for Arrhenius analysis. A control sample, not annealed, is also analyzed to assess background levels.

SIMS is a powerful analytical technique for determining elemental and isotopic distributions in solids [19,20]. An ION-TOF TOF-SIMS V spectrometer is used for P-depth profiling and 3D tomography of P diffused samples. A Cs^+ ion sputtering beam with an energy of 3 keV and current of 25 nA is scanned over an area of 250×250 μm. Secondary ions for analysis are created by a three-lens 30-keV BiMn ion gun. Two different measurement modes are used. Depth profiles are collected with a high data density with a Bi^+ beam operated in bunched mode with a 12-ns pulse width and 1-pA analysis current scanned over a 50-μm area; a primary-ion-beam dose density of 5×10^{11} ions/cm^2 is used for most of these profiles. In some cases, profiles are collected using the bunched Bi^+ beam (1-pA pulsed primary-ion current) at a dose density of 1×10^{14} ions/cm^2, matching the dosage used during 3D tomography and imaging to enable a lower background for phosphorous. 3D tomography is completed with 100-nm lateral resolution using a $Bi_3{}^{++}$ primary-ion beam cluster (100-ns pulse width, 0.1-pA pulsed beam current), a 25×25 μm area is sampled with a 256:256 primary-beam raster, and a primary-ion beam dosage of 1×10^{14} ions/cm^2 for each imaging cycle. Crater depth is determined by optical interference light microscopy after SIMS measurements to convert the SIMS sputter time scale to a sputter depth scale. Both pure phosphorus ions (P^-) and phosphate ($PO_2{}^-$) ions are considered for diffusion analysis; however, only the P^- signal is used for quantitative analysis.

TABLE I. Diffusion temperatures and times.

Thermocouple temperature [°C]	Time [h]	Expected bulk-diffusion length ($2\sqrt{D_b t}$) [nm]
561	32	370
585	30	530
609	7	370
633	7	520
680	2	520

Bulk diffusion is fit using the solution to the one-dimensional (1D) diffusion equation known at Fick's second law for a constant diffuser source,

$$C[z,t] = C_0 \mathrm{erfc}\left[\frac{z}{2\sqrt{D_b t}}\right], \tag{1}$$

where C is the time- and depth-dependent concentration of the diffuser, C_0 is the surface concentration (solubility), *erfc* is the complementary error function, and D_b is the bulk-diffusion coefficient. Diffusion coefficients can often be described by the Arrhenius relation $D[T] = D_0 \exp[-(E_A/k_B T)]$, where the activation energy (E_A) and prefactor (D_0) are correlated with a single diffusion mechanism [21]. The Smoluchowski solution for an isolated dislocation core [22] is used to assess the possibility of dislocation diffusion, whereas a two-error function model is used to evaluate two separate bulk-diffusion mechanisms.

Polycrystalline diffusion profiles are analyzed using the Le Claire method with Chung and Wuensch modifications [23]. The slope of the normalized intensity plotted versus the unitless parameter $\eta^{6/5}$ is used to extract the GB diffusion coefficient (D_{GB}):

$$\frac{\partial \mathrm{In}[C/C_0]}{\partial \eta^{6/5}} = -\left[\left(\frac{\partial D_{\mathrm{GB}}}{\sqrt{D_b^3 t}}\right) 10^{-A}\right]^{-B}. \tag{2}$$

This solution is valid for $1 \leq \delta\, D_{\mathrm{GB}}/\sqrt{D_b^3\, t} \leq 10^5$, where δ is the GB width (5 nm is used as is common in cubic systems) [21]. The Fisher-isolated-GB solution is used to establish initial parameter values in the fitting algorithm [24].

Ab initio band-structure and total-energy calculations are performed using density-functional theory [25,26], which has been implemented in the VASP code [27,28]. The frozen-core projected augmented wave approach is used to include electron and core interactions [29]. The Heyd-Scuseria-Ernzerhof hybrid functional is used to correct band-gap error [30]. The defect calculations are performed

within a 64-atom supercell. All the atoms in the supercell are relaxed until the forces on each atom are less than 0.05 eV/Å. $2 \times 2 \times 2$ Monkhorst-Pack special k-point meshes and the Gaussian smearing method (SIGMA = 0.02) are used to calculate the total energy, which ensures convergence to within 0.1 eV using an energy cutoff of 300 eV. The method in Ref. [31] is used to calculate defect properties. The calculated lattice constant of pure CdTe is 6.58 Å with a band gap of 1.49 eV using the Heyd-Scuseria-Ernzerhof functional with the default exchange parameters ($\alpha = 0.25$), which agrees well with experimental CdTe data [32].

III. RESULTS AND DISCUSSION

Figure 1(a) shows the experimental P distribution as a function of depth for *sX* samples exposed to three different *ex situ* process conditions. There is a slow bulk-diffusion profile for about 500 nm, which is fit well by an erfc function and consistent with earlier work for both diffusion coefficients and surface concentrations. The control sample did not show P above the detection limit. Lateral two-dimensional (2D) P-intensity slices are shown for several depths in Fig. 1(c). The nonzero and uniform P intensity observed at depths beyond 500 nm [see Fig. 1(c)(iii)] suggests that there is a secondary diffusion mechanism in the *sX* samples. To better understand the secondary—and substantially faster—diffusion, 1D profiles are measured again on the *sX* samples at higher primary ion beam dosage. This improves the detection limit, but results in lower data density [see Fig. 1(b)]. The same slow bulk behavior is observed for the first 500 nm; but with the improved detection limit, the fast diffusion tail indicating deep P penetration is clearly observed.

Polycrystalline samples exhibited the same diffusion shape as the single crystals for the first 500 nm [Fig. 2(a)]. This is followed by deep P penetration beyond 500 nm. The bulk diffusion near the surface is enhanced somewhat compared to the *sX* samples. The Hart equation, $D_{ef} = g\, D_{gb} + (1 - g) D_b$, can be used to interpret the effective bulk-diffusion coefficient measured from bulk and GB diffusion near the top surface with the surface area ratio $g = (gb$ surface area/bulk surface area) [33]. Using the approximate grain size, bulk-diffusion coefficient extracted from the *sX* samples, and the GB diffusion coefficient extracted using the Le Claire–Chung method (see Supplemental Material [34]), the effective diffusion

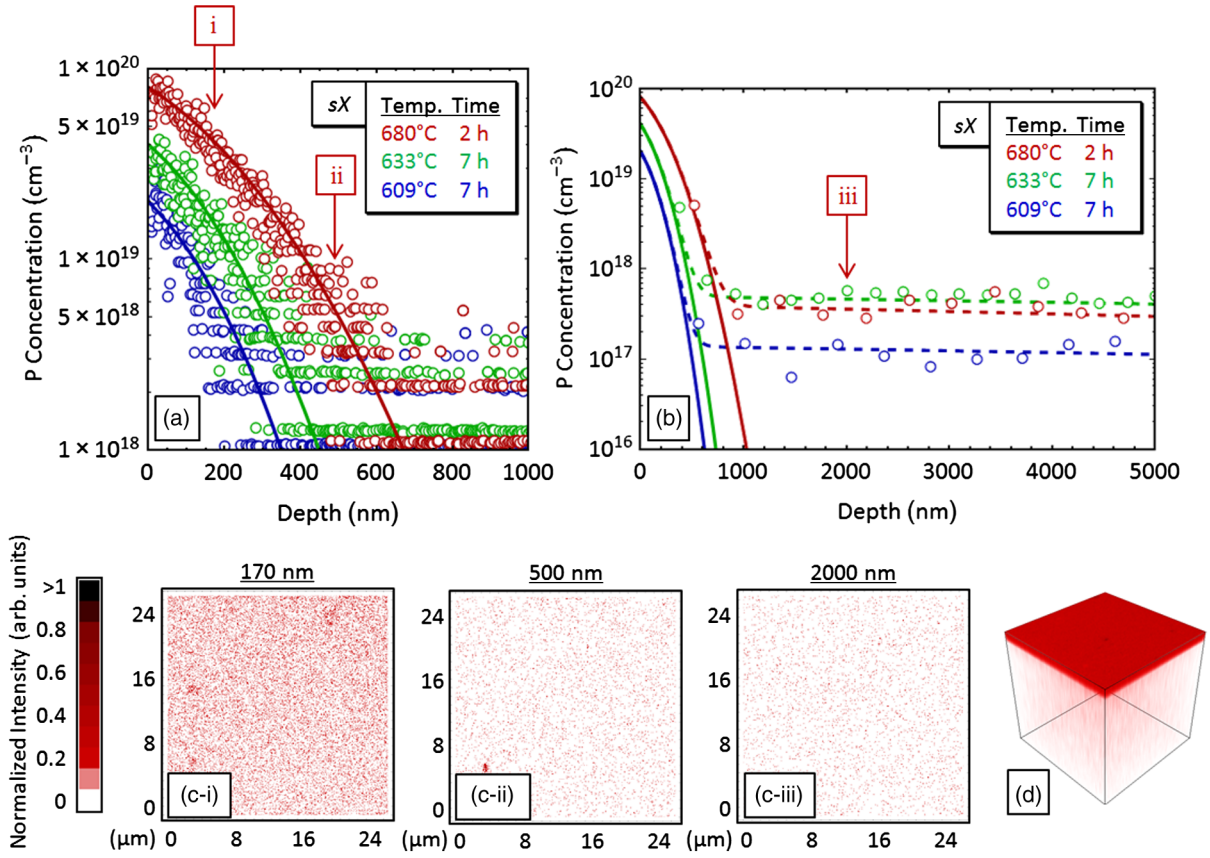

FIG. 1 (a) 1D phosphorus concentration profiles from the TOF-SIMS system for three representative *sX* samples (open circles) and associated *erfc* fits (solid lines). (b) 1D profiles taken with higher primary-ion-beam dosage but lower data density and associated *erfc* fits from (a) (solid lines) and two *erfc* fits (dashed lines). (c) Lateral 2D P-intensity slices taken at three depths for the *sX* 680 °C, 2-h sample. (d) 3D TOF-SIMS P-intensity tomography rendering ($25 \times 25 \times 2.2$ μm) for the *sX* 680 °C, 2-h sample.

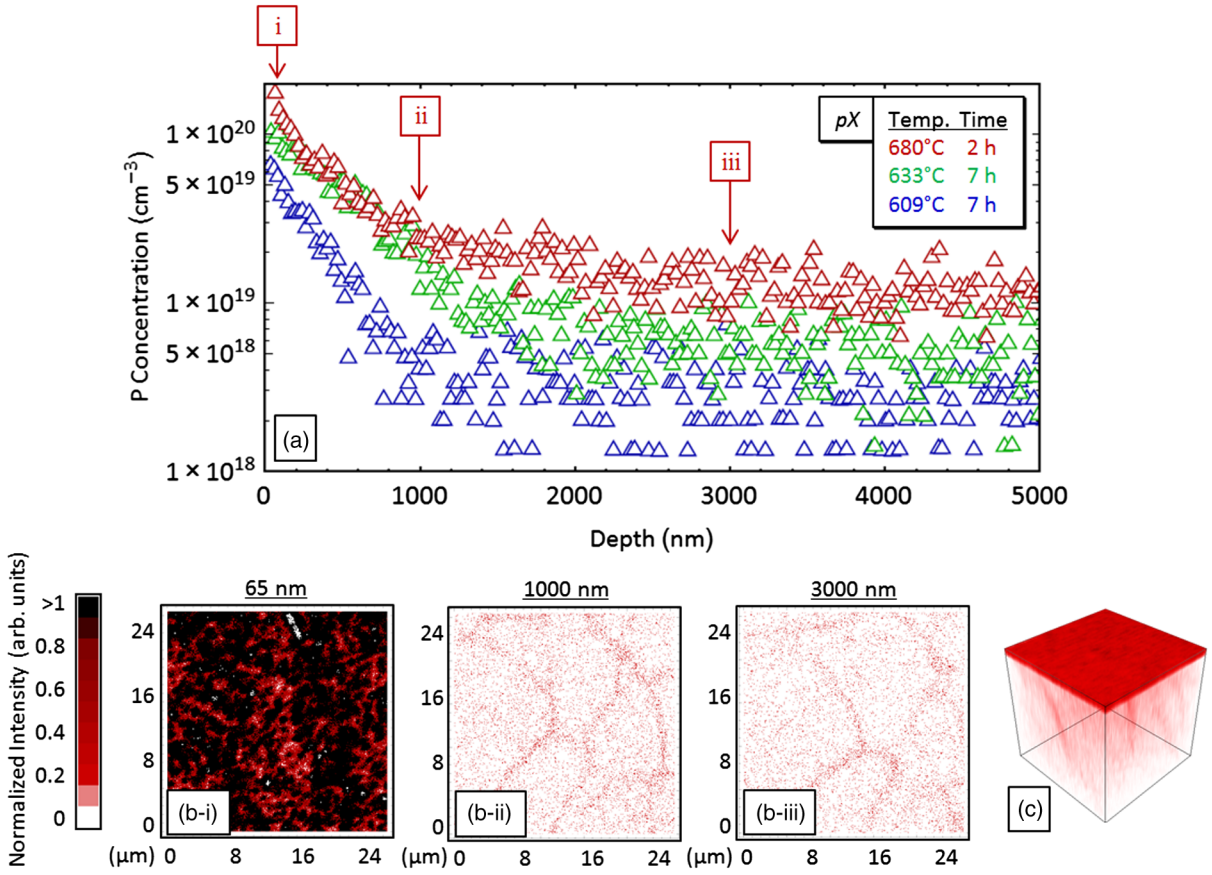

FIG. 2. (a) 1D phosphorus concentration profiles from the TOF-SIMS system for three representative *pX* samples (open triangles). (b) Lateral 2D P-intensity slices taken at three depths for the *pX* 680 °C, 2-h sample. (c) 3D TOF-SIMS P-intensity tomography rendering ($25 \times 25 \times 16.7$ μm) for the *pX* 680 °C, 2-h sample.

coefficients calculated using the Hart equation are consistent with the measured diffusion profiles.

The lateral 2D P-intensity slices [Fig. 2(c)] yield two important insights into P diffusion in *pX* CdTe. First, there is clear enhancement of the P signal at GBs. This enhanced P is directly correlated with electron backscatter diffraction GB maps [35]. This GB diffusion allows P to penetrate deep into *pX* films and confirms that GB diffusion is a significant aspect of the P concentration measured in 1D *pX* profiles shown in Fig. 2(a). The GB P concentration varies with diffusion conditions, but is generally between 10^{19} and 10^{20} cm^{-3}, which is similar to the measured surface concentration. The second insight from the lateral 2D P-intensity slices is that P is present in the center of large grains at depths significantly greater than 500 nm [see Fig. 2(c)(iii)]. If GBs and the previously discussed slow bulk diffusion are the only two mechanisms for P incorporation, there should be only background levels of P detected in the grain cores. Similar to the *sX* slices in Fig. 1(c), the presence of nonzero concentrations of P in the center of these grains suggests that there is another diffusion mechanism facilitating P diffusion in CdTe.

Interestingly, earlier experiments on single crystals revealed a fast diffusion component but it was not given much attention [17,18]. Hoonnivathana *et al.* suggested that it may be related to GBs or dislocations. However, GBs are not present in our *sX* samples; so, in this case, they are not responsible for the fast bulk-diffusion component. Dislocation diffusion coefficients and densities can be found approximately using Smoluchowski's dislocation pipe solution mentioned earlier [22]. However, when the measured profiles are analyzed with this method, the dislocation densities need to be on the order of 10^8 cm^{-2} and the diffusion coefficients need to be 3–4 orders of magnitude higher than even the GB diffusion coefficients. Although it is possible that the *sX* near-surface dislocation density could be quite high (about 10^7 cm^{-2}) due to polishing damage, the dislocations are not expected to penetrate more than several micrometers. Bulk dislocation density is estimated to be less than 10^5 cm^{-2} by Nippon. Consequently, it is unlikely that the *sX* P concentration beyond 500 nm can be described by the dislocation diffusion speculated in previous work [18,35]. It is more likely that there is a second bulk-diffusion mechanism as mentioned above. In support of

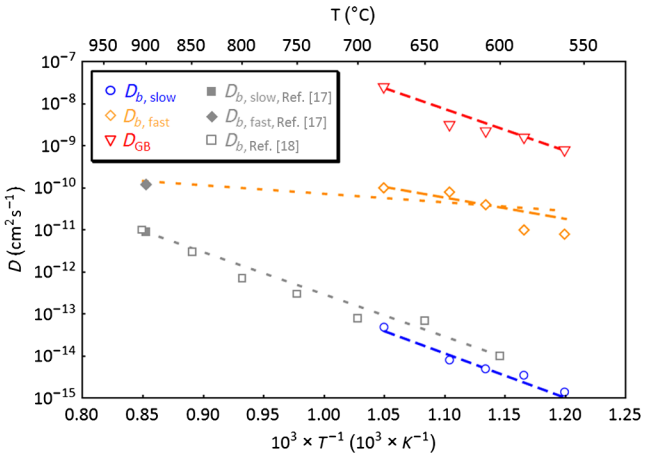

FIG. 3. Arrhenius plots for diffusion coefficients (D) for associated diffusion mechanisms discussed in text. Dashed lines are Arrhenius temperature dependence fits from our data. Dotted lines are Arrhenius temperature dependence fits including reference data. Fit parameter details are summarized in Table II.

this, the combination of two erfc functions representing two bulk-diffusion mechanisms provides a good fit for the *sX* P distributions [see Fig. 1(b)]. Figure 3 shows an Arrhenius plot for the diffusion coefficients and comparisons with earlier work; the fit parameters are given in Table II.

To understand P-related defects in CdTe and diffusion properties that may describe the experimental observations, we perform atomistic *ab initio* theoretical calculations. Figure 4(a) shows our calculated intrinsic and P-related defect formation energies as functions of Fermi energy in CdTe under Cd-rich conditions. These defects form the basis for experimental P incorporation. The calculations suggest that the dominant P-related defects are P on Te sites (P_{Te}) as they have the lowest formation energies. If P directly substitutes Te at the tetragonal sites surrounded by four Cd atoms, P_{Te} defects act as negatively charged acceptors (P_{Te}^{-}, solid red line). If P_{Te} forms AX centers by structure distortions, P_{Te} defects act as positively charged donors (P_{Te}^{+}, dashed red line) [36]. However, once the Te vacancies are consumed, P will form interstitial defects by going to T_c sites (surrounded by four Cd atoms, $P_{i,Tc}$), T_a sites (surrounded by four Te atoms, $P_{i,Ta}$), or split interstitial sites ($P_{i,spl}$), as shown in Fig. 4. Although the formation energies of P interstitial defects are significantly higher than that of the P substitutional defects, the amount of P interstitial defects can be large if P concentrations are high. Diffusion is governed not only by the defect densities which are determined by defect formation energy, but also diffusion energy barriers for the atomic configurations formed as impurities move through the lattice. Consequently, CdTe P diffusion can be through substitutional and interstitial defects. For the substitutional defects, a P_{Te} defect first dissociates to a P interstitial and Te vacancy, then diffuses to form another P_{Te} defect by either kicking a Te atom off or filling a nearby Te vacancy (the possibility is small since we assume all the Te vacancies are already consumed). To maintain the charge balance requirement before and after dissociation, we propose the following dissociation reaction: $P_{Te}^{+} \rightarrow P_{i,spl}^{-} + V_{Te}^{2+}$. Other dissociations are expected to be less important due to the limitation of charge balance or the larger dissociation energy cost. Figure 4(b) shows the structural model of how an AX center defect P_{Te}^{+} dissociates to V_{Te}^{2+} and P_i^{-} during this diffusion process. We find from Fig. 4(a) that the total energy is increased by 1.95 eV after the dissociation and thus, the energy barrier to form a $P_{i,spl}$ and V_{Te} from P_{Te} must be even greater than 1.95 eV. This energy correlates well with the slow bulk diffusion of P measured experimentally. For P interstitial defects, we consider the split interstitials due to the smaller formation energies compared to other interstitial defects. We find that the $P_{i,spl}$ defects can diffuse following a mechanism containing one kick-out step and two rotational steps with diffusion barriers between 0.4 and 0.8 eV (see Fig. S4 in Ref. [34]). This means that a $P_{i,spl}$ can diffuse to an adjacent $P_{i,spl}$ quickly once the defect is formed. This diffusion mechanism is consistent with the fast bulk P diffusion experimentally observed. Note that for a specified diffusion path, usually the largest energy barrier is dominant and will correspond to the experimental Arrhenius activation energy [37]. The GB diffusion activation energy is equivalent to the slow bulk activation energy, so it is plausible that P moving through Te sites is the primary GB diffusion mechanism. Faster GB diffusion

TABLE II. Arrhenius parameters for measured P diffusion mechanisms compared to theoretical predictions and reference data.

	D_0 ($\text{cm}^2\ \text{s}^{-1}$)	E_A (eV)	
Mechanism	Fit	Fit	Theoretical prediction
Slow bulk	$4.86 \pm 20 \times 10^{-3}$	2.10 ± 0.34	>1.95
Fast bulk	$2.15 \pm 4 \times 10^{-5}$	1.00 ± 0.15	0.4 to 0.8
GB	$6.61 \pm 17 \times 10^{2}$	1.97 ± 0.20	>1.95
Slow bulk Ref. [18]	$3.35 \pm 3.6 \times 10^{-3}$	1.99 ± 0.10	…
Fast bulk and Ref. [17]	$7.66 \pm 12 \times 10^{-9}$	0.40 ± 0.07	0.4 to 0.8

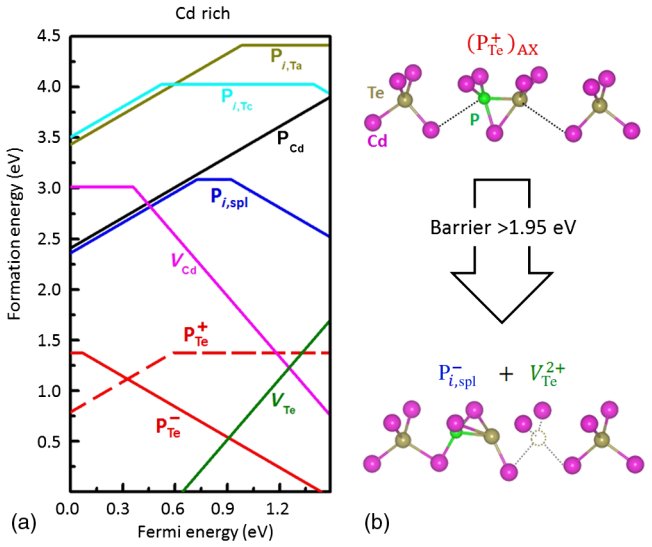

FIG. 4. (a) Calculated formation energies of P-related defects as functions of Fermi energy (referenced to the valence band maximum) under Cd-rich conditions. (b) Structural model to show how the AX center defect P_{Te}^{+} can dissociate to V_{Te}^{2+} and P_i^{-} with an energy barrier greater than 1.95 eV (green balls are P atoms, pink balls are Cd atoms, and gold balls are Te atoms).

rates than the bulk can be the result of a much higher density of V_{Te} sites at GBs. Table II indicates that the theoretical predictions are in reasonable agreement with the experimental results.

The fast bulk-diffusion mechanism will allow for deep incorporation of P at relatively low temperatures, but the high formation energy of the $P_{i,spl}$ defect limits the total P concentrations at those depths. One route that may enable higher concentrations of P to deeply penetrate CdTe, would be to perform the diffusion process in Te-rich conditions where the formation energy of the $P_{i,spl}$ defect is lower and the V_{Te} density is also much lower due to a higher formation energy (Fig. S3 [34]). Once the P is incorporated, a subsequent anneal to move the P to Te sites can allow for high hole densities to be achieved throughout *sX* and *pX* CdTe material.

IV. CONCLUSIONS

Experimental P diffusion profiles and theoretical calculations indicate that there are two bulk-diffusion mechanisms controlling P dopant incorporation in CdTe. The first mechanism, associated with P_{Te}, has a low formation energy but a high diffusion barrier. This mechanism is manifested by a high dopant concentration near the surface but shallow penetration. The second component associated with P interstitials is correlated with a low concentration but deep penetration. Furthermore, GB diffusion of P is 5 orders of magnitude greater than the slow bulk diffusion of P. The fast bulk-diffusion mechanism is critical because it provides a route to incorporate P deep in single crystals and throughout the grains of *pX* films. This deep-penetrating P provides the potential to overcome longstanding doping limits in CdTe photovoltaics and can be useful in other semiconductor device applications.

ACKNOWLEDGMENTS

This work is supported by the U.S. Department of Energy (DOE), Office of Energy Efficiency and Renewable Energy, under Contract No. DE-AC36-08GO28308.

[1] J. Ma, D. Kuciauskas, D. Albin, R. Bhattacharya, M. Reese, T. Barnes, J. V. Li, T. Gessert, and S. Wei, Dependence of the Minority-Carrier Lifetime on the Stoichiometry of CdTe Using Time-Resolved Photoluminescence and First-Principles Calculations, Phys. Rev. Lett. **111**, 067402 (2013).

[2] C. Corwine, A. Pudov, M. Gloeckler, S. Demtsu, and J. Sites, Copper inclusion and migration from the back contact in CdTe solar cells, Sol. Energy Mater. Sol. Cells **82**, 481 (2004).

[3] D. S. Albin, in *Proeedings of SPIE 7048: Reliability of Photovoltaic Cells, Modules, Components, and Systems, San Diego, 2008* (SPIE, San Diego, 2008).

[4] J. N. Duenow, J. M. Burst, D. S. Albin, D. Kuciauskas, S. W. Johnston, R. C. Reedy, and W. K. Metzger, Single-crystal CdTe solar cells with V_{oc} greater than 900 mV, Appl. Phys. Lett. **105**, 053903 (2014).

[5] M. Nardone and D. S. Albin, Degradation of CdTe solar cells: simulation and experiment, IEEE J. Photovoltaics **5**, 962 (2015).

[6] J. Chamonal, E. Molva, and J. Pautrat, Identification of Cu and Ag acceptors in CdTe, Solid State Commun. **43**, 801 (1982).

[7] D. Kuciauskas, P. Dippo, A. Kanevce, Z. Zhao, L. Cheng, A. Los, M. Gloeckler, and W. K. Metzger, The impact of Cu on recombination in high voltage CdTe solar cells, Appl. Phys. Lett. **107**, 243906 (2015).

[8] J. M. Burst, S. B. Farrell, D. S. Albin, E. Colegrove, M. O. Reese, J. N. Duenow, D. Kuciauskas, and W. K. Metzger (unpublished).

[9] M. A. Green and K. Emery, Solar cell efficiency tables (version 2), Prog. Photovoltaics **1**, 225 (1993).

[10] M. A. Green, K. Emery, Y. Hishikawa, W. Warta, and E. D. Dunlop, Solar cell efficiency tables (version 45), Prog. Photovoltaics **23**, 1 (2015).

[11] M. Gloeckler, I. Sankin, and Z. Zhao, CdTe solar cells at the threshold to 20% efficiency, IEEE J. Photovoltaics **3**, 1389 (2013).

[12] First Solar, http://www.firstsolar.com/Solutions/Utility-Scale-Generation.aspx.

[13] J. M. Burst, J. N. Duenow, D. S. Albin, E. Colegrove, M. O. Reese, J. A. Aguiar, C.-S. Jiang, M. K. Patel, M. M. Al-Jassim, D. Kuciauskas, S. Swain, T. Ablekim, K. G. Lynn, and W. K. Metzger, CdTe solar cells with open-circuit voltage breaking the 1 V barrier, Nat. Energy **1**, 16015 (2016).

[14] F. Selim and F. Kroger, The defect structure of phosphorus-doped CdTe, J. Electrochem. Soc. **124**, 401 (1977).

[15] E. Molva, J. Pautrat, K. Saminadayar, G. Milchberg, and N. Magnea, Acceptor states in CdTe and comparison with ZnTe. General trends, Phys. Rev. B **30**, 3344 (1984).
[16] S. Wei and S. B. Zhang, Chemical trends of defect formation and doping limit in II-VI semiconductors: The case of CdTe, Phys. Rev. B **66**, 155211 (2002).
[17] R. Hall and H. Woodbury, The diffusion and solubility of phosphorus in CdTe and CdSe, J. Appl. Phys. **39**, 5361 (1968).
[18] E. Hoonnivathana, E. Jones, I. Viney, and L. Duckers, Diffusion of phosphorus in CdTe, J. Electron. Mater. **27**, 610 (1998).
[19] R. A. De Souza and M. Martin, Probing diffusion kinetics with secondary ion mass spectrometry, MRS Bull. **34**, 907 (2009).
[20] R. G. Wilson, F. A. Stevie, and C. W. Magee, *Secondary Ion Mass Spectrometry: A Practical Handbook for Depth Profiling and Bulk Impurity Analysis* (Wiley, New York, 1989).
[21] I. Kaur, Y. Mishin, and W. Gust, *Fundamentals of Grain and Interphase Boundary Diffusion* (Wiley, West Sussex, 1995).
[22] R. Smoluchowski, Theory of grain boundary diffusion, Phys. Rev. **87**, 482 (1952).
[23] Y. Chung and B. J. Wuensch, An improved method, based on Whipple's exact solution, for obtaining accurate grain-boundary diffusion coefficients from shallow solute concentration gradients, J. Appl. Phys. **79**, 8323 (1996).
[24] J. Fisher, Calculation of diffusion penetration curves for surface and grain boundary diffusion, J. Appl. Phys. **22**, 74 (1951).
[25] P. Hohenberg and W. Kohn, Inhomogeneous electron gas, Phys. Rev. **136**, B864 (1964).
[26] W. Kohn and L. Sham, Self-consistent equations including exchange and correlation effects, Phys. Rev. **140**, A1133 (1965).
[27] G. Kresse and J. Furthmülle, Efficient iterative schemes for *ab initio* total-energy calculations using a plane-wave basis set, Phys. Rev. B **54**, 11169 (1996).
[28] G. Kresse and J. Furthmüller, Efficiency of *ab-initio* total energy calculations for metals and semiconductors using a plane-wave basis set, Comput. Mater. Sci. **6**, 15 (1996).
[29] G. Kresse and D. Joubert, From ultrasoft pseudopotentials to the projector augmented-wave method, Phys. Rev. B **59**, 1758 (1999).
[30] J. Heyd, G. E. Scuseria, and M. Ernzerhof, Hybrid functionals based on a screened Coulomb potential, J. Chem. Phys. **118**, 8207 (2003).
[31] S.-H. Wei, Overcoming the doping bottleneck in semiconductors, Comput. Mater. Sci. **30**, 337 (2004).
[32] *Landolt-Bornstein: Numerical data, and functional relationships in science, and technology*, edited by O. Madelung, M. Schulz, and H. Weiss (Springer, Verlag, 1982), Vol. 17b.
[33] E. Hart, On the role of dislocations in bulk diffusion, Acta Metall. **5**, 597 (1957).
[34] See Supplemental Material at http://link.aps.org/supplemental/10.1103/PhysRevApplied.5.054014 for additional figures and discussion.
[35] E. Colegrove, D. S. Albin, H. Guthrey, S. Harvey, J. Burst, H. Moutinho, S. Farrell, M. Al-Jassim, and W. K. Metzger, in *Proceedings of the IEEE 42nd Photovoltaic Specialist Conference (PVSC), 2015* (IEEE, New Orleans, 2015).
[36] J. Yang, W. Yin, J. Park, J. Burst, W. K. Metzger, T. Gessert, T. Barnes, and S. Wei, Enhanced *p*-type dopability of P and As in CdTe using non-equilibrium thermal processing, J. Appl. Phys. **118**, 025102 (2015).
[37] J.-H. Yang, J.-S. Park, J. Kang, and S.-H. Wei, First-principles multiple-barrier diffusion theory: The case study of interstitial diffusion in CdTe, Phys. Rev. B **91**, 075202 (2015).